**Supporting information for**

# Soft non-porous separator and its effectiveness in stabilizing Li metal anode cycling at 10 mA/cm$^2$ observed in-situ in a capillary cell

Kai Liu,[1,2] Peng Bai,[3] Martin Z. Bazant,[3, 4] Chang-An Wang,[1, *] Ju Li[2,5,*]

[1] State Key Lab of New Ceramics and Fine Processing, School of Materials Science and Engineering, Tsinghua University, Beijing 100084, P. R. China.

[2] Department of Nuclear Science and Engineering, Massachusetts Institute of Technology, Cambridge, Massachusetts 02139, USA.

[3] Department of Chemical Engineering, Massachusetts Institute of Technology, Cambridge, Massachusetts 02139, USA.

[4] Department of Mathematics, Massachusetts Institute of Technology, Cambridge, Massachusetts 02139, USA.

[5] Department of Materials Science and Engineering, Massachusetts Institute of Technology, Cambridge, Massachusetts 02139, USA.

* Correspondence to: wangca@mail.tsinghua.edu.cn (C. Wang) or liju@mit.edu (J. Li)

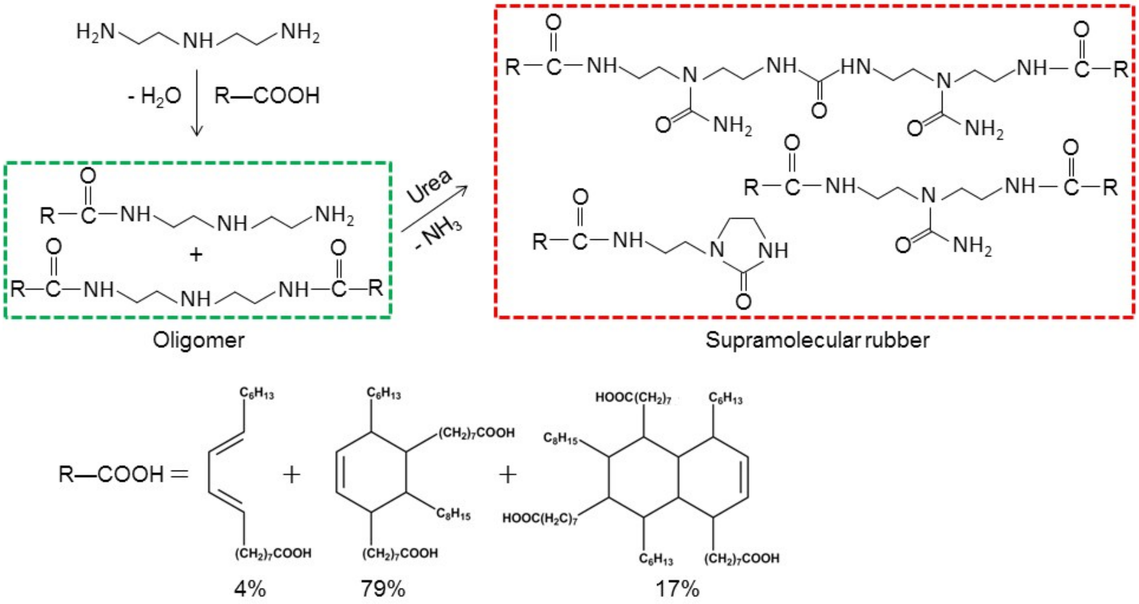

**Fig. S1** Synthesis pathway and the molecule structures.

It should be mentioned that reaction of only one –COOH group in fatty dimmer acid R-COOH is showed, however, there are two or three –COOH groups in most of R-COOH molecules, and all of them can react with DETA resulting in cross-linked supramolecules.

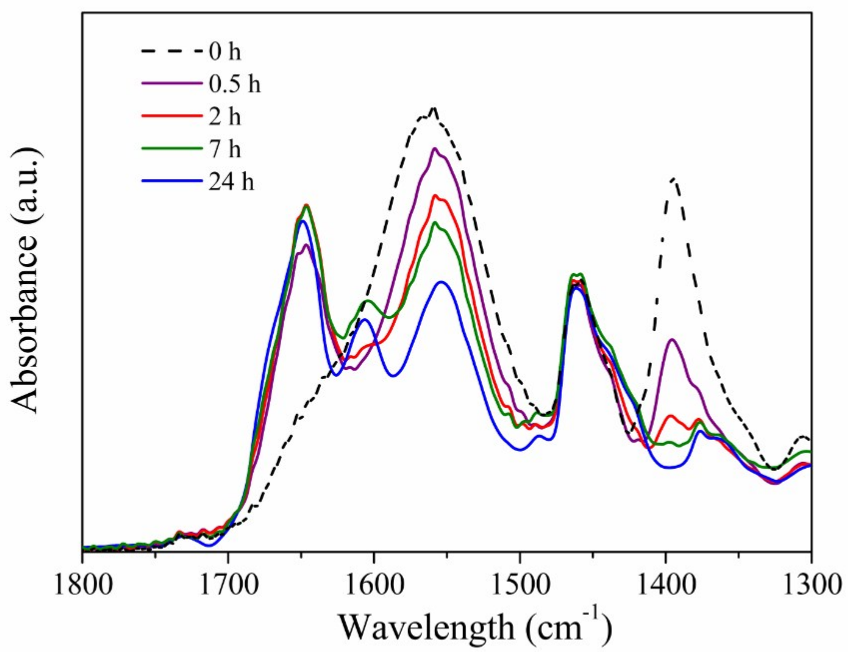

**Fig. S2** FTIR spectra of the synthesis oligomer after 0 h, 0.5 h, 2 h, 7 h and 24 h of reaction. (Instrument: Vertex70v, Bruker)

While reaction time increases, the $\upsilon s_{COO-}$ and $\delta_{NH}$ signals at 1394 and 1550 cm$^{-1}$ decreases, and the $\upsilon_{CO}$ amide signal at 1645 cm$^{-1}$ appears right after the reaction begins. This result is well consistent with the result reported in reference [L. Leibler et al, Journal of Polymer Science: Part A: Polymer Chemistry, 2008, 46, 7925-7936], which confirm the reaction between –COOH groups in fatty dimmer acid and –$NH_2$ groups in DETA.

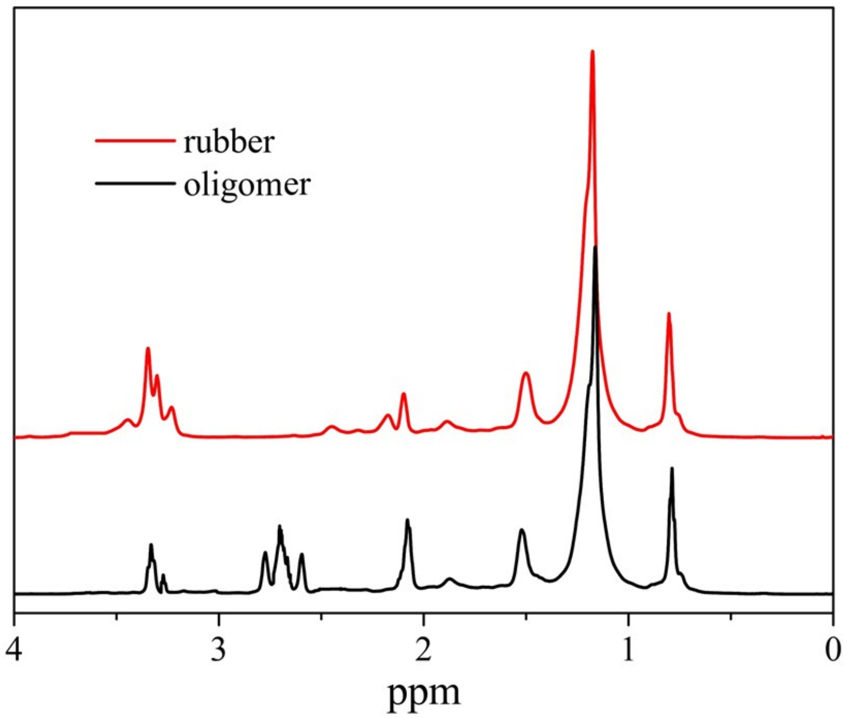

**Fig. S3** NMR of the oligomer and the rubber. (Instrument: Varian Mercury 400 NMR spectrometer)

The peaks at 2.6 and 2.8 corresponds to the protons on $CH_2$ connected to primary amines. The peaks at 2.7 corresponds to the protons on -$CH_2$ groups connected to secondary amines. Upon reaction, as can be seen in the spectra of the rubber, all the three peeks disappeared, indicating that the primary amine groups and secondary amine groups were converted into urea. This result is also consistent with the results in references [L. Leibler et al, Journal of Polymer Science: Part A: Polymer Chemistry, 2008, 46, 7925-7936] and [Z. Bao et al, Nature Chemistry, 2013, 5, 1042-1048].

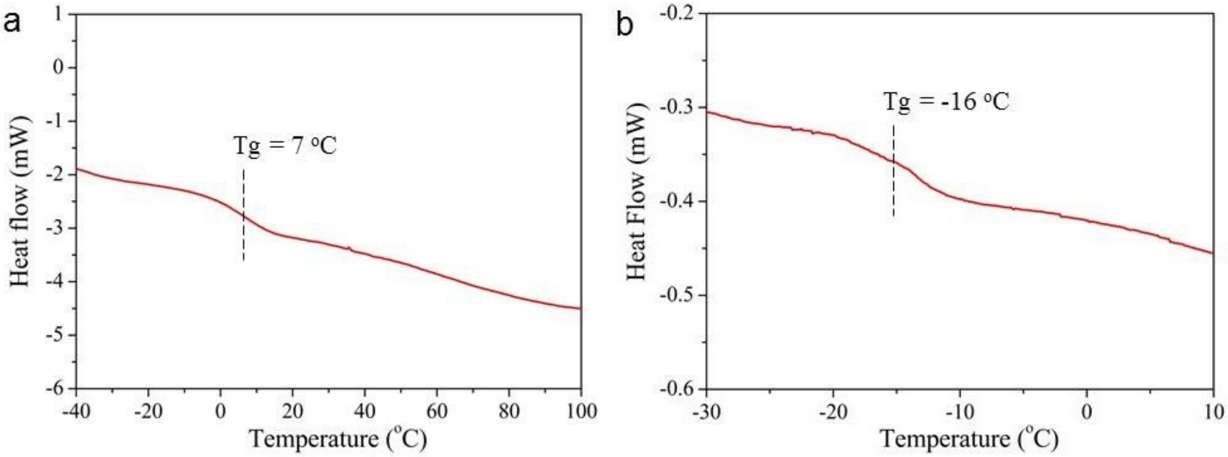

**Fig. S4** Differential scanning calorimetry (DSC) traces of the rubber separator before swelling (a) and after swelling (b). The experiment was conducted at a heating rate of 10 °C/min under $N_2$ atmosphere. (Instrument: DSC Q2000, TA Instruments)

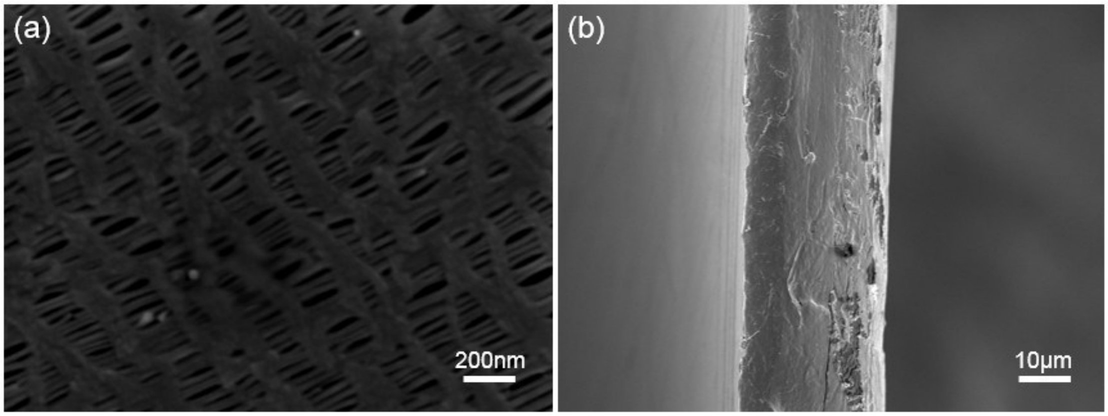

**Fig. S5** SEM images of the commercial porous PP separator (Celgard 2400). (a) Surface, top view; (b) cross section, side view.

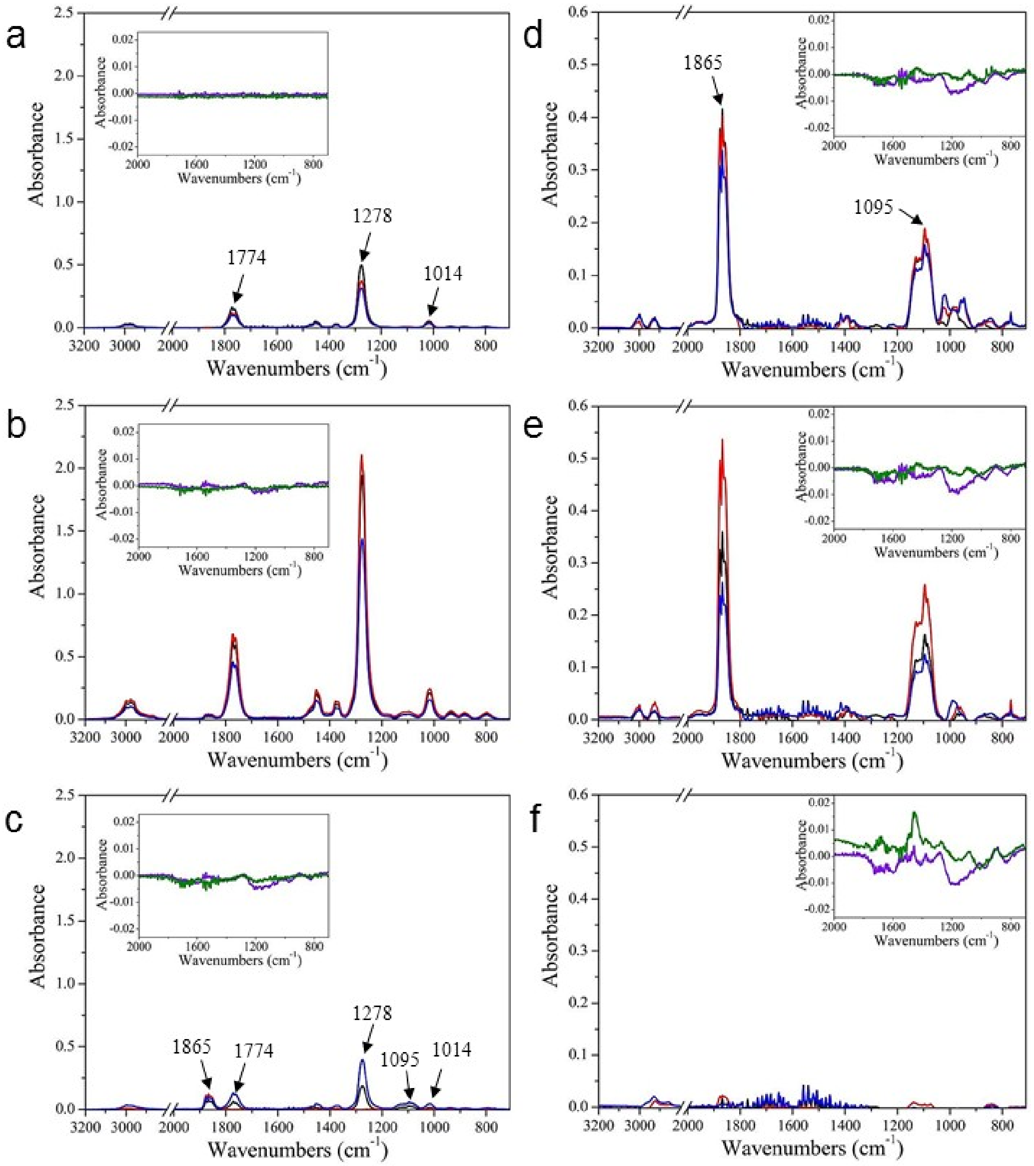

**Fig. S6** FTIR Spectra of the vapor come out from the samples at different temperatures. (a) 50 $^{o}$C; (b) 100 $^{o}$C; (c) 150 $^{o}$C; (d) 220 $^{o}$C; (e) 300 $^{o}$C; (f) 450 $^{o}$C. For all the images, black line: 1 M $LiPF_6$ in EC/MEC (3:7 by volume) liquid electrolyte; red line: the liquid electrolyte swelled celgard 2400; blue line: the liquid electrolyte swelled rubber separator; insert purple line: dry (pristine) celgard 2400; insert green line: dry (pristine) rubber membrane. (Instrument: Vertex70v, Bruker)

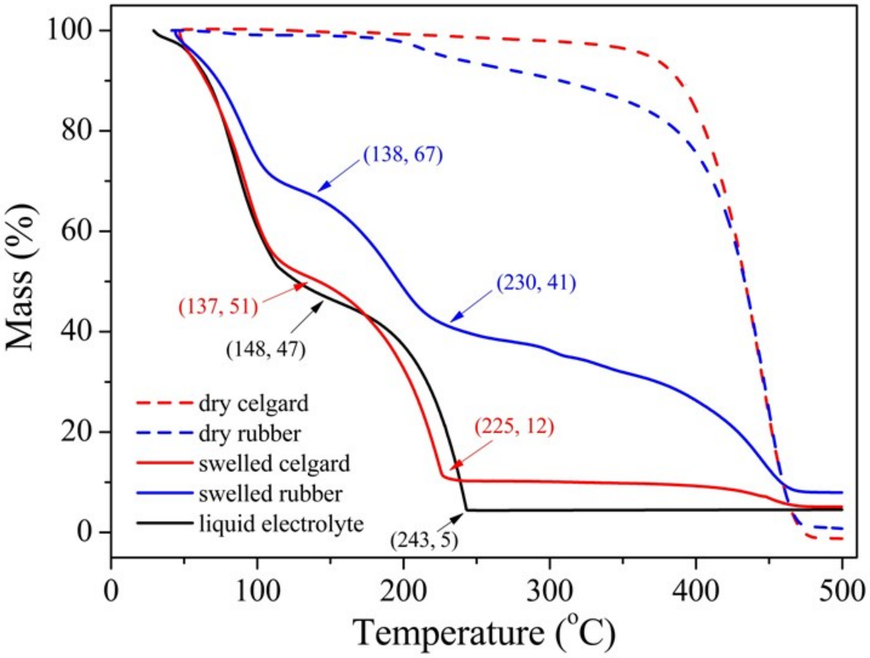

**Fig. S7** Thermogravimetric curves of the 1 M $LiPF_6$ in EC/MEC (3:7 by volume) liquid electrolyte and separators. Temperature range: room temperature to 500 °C; heating rate: 5 °C/min; atmosphere: Ar. (Instrument: QMS 403C, Netzsch)

The thermogravimetric curve of the liquid electrolyte can be divided into three sections: section 1) room temperature to 148 °C, in which the whole mass loss is 53%; section 2) 148 °C to 243 °C, and the mass loss is 42%; section 3) 243 °C to 500 °C, no mass loss. According to the composition of the liquid electrolyte and the densities of the components, we can calculate that the mass percentage of the EMC, which has much lower boiling point than EC and should evaporate first, is ~55%, very close to the mass loss in section 1. From Figure S6 we can see, at 50 °C and 100 °C, the peeks of the liquid electrolyte's spectra are well consistent with the peeks of chain carbonate [http://webbook.nist.gov/cgi/cbook.cgi?ID=C616386&Units=SI&Type=IR-SPEC&Index=1#IR-SPEC; http://webbook.nist.gov/cgi/cbook.cgi?ID=C105588&Units=SI&Type=IR-SPEC&Index=1#IR-SPEC], so we can conclude that in section 1, the main vapor came out is EMC. In section 2, the vapor's FTIR peeks (Figure S6(d)) can be well identified as EC [http://webbook.nist.gov/cgi/cbook.cgi?ID=C96491&Units=SI&Type=IR-SPEC&Index=0#IR-SPEC]. However, the mass loss in section 2 (42%) is higher than the mass percentage of EC in the liquid electrolyte (32%). The mass loss different could come from the loss of $PF_5$ gas generated from the decomposition of $LiPF_6$. The ratio between the mass loss in section 1 and section 2 is 53/42=1.26. In section 3, there was no mass loss, but FTIR signals could still be observed, which may due to the evaporation of EC condensed inside the connecting tubes (kept at 200 $^{o}$C during the whole test) of the instruments. The final mass remained in section 3 (5%) should be generally positively related to to the mass percentage of $LiPF_6$ salt. In summary, these TG-FTIR results can roughly and effectively confirm the composition of the liquid electrolyte.

Based on the analysis of the liquid electrolyte TG-FTIR results, the behaviour of Celgard 2400 and the rubber samples under heating can be well understood. For the swelled Celgard separator, its TG curve can also be divided into the same 3 sections (demarcation points are 137 and 225 $^{o}$C). The ratio between the mass loss in section 1 and section 2 is 49/39=1.26, the same as the results of the liquid electrolyte sample. The FTIR signals at different temperatures are also highly similar to liquid eletrolyte's signals. For the swelled rubber separator, the demarcation points of its TG curve are 138 and 230 $^{o}$C, and the ratio between the mass loss in section 1 and section 2 is 33/26=1.27, and the FTIR signals are highly similar as well. These results indicate that the liquid electrolytes imbibed into both two kind of separators have solvents with the same composition as the bulk liquid electrolyte's solvent.

The difference of the final masses remained at 500 $^{o}$C between swelled and dry samples are positively relevant to the mass percentage of $LiPF_6$ salt uptook into the separator. For Celgard and the rubber samples, the differences are 6% and 7% respectively. Considering the mass percentage of liquid electrolyte imbibed (~90% and ~60% for Celgard and rubber, respectively), it seems that the liquid electrolyte imbibed into the rubber separator has a much higher $LiPF_6$ salt concentration, but further investigation is needed to confirm.

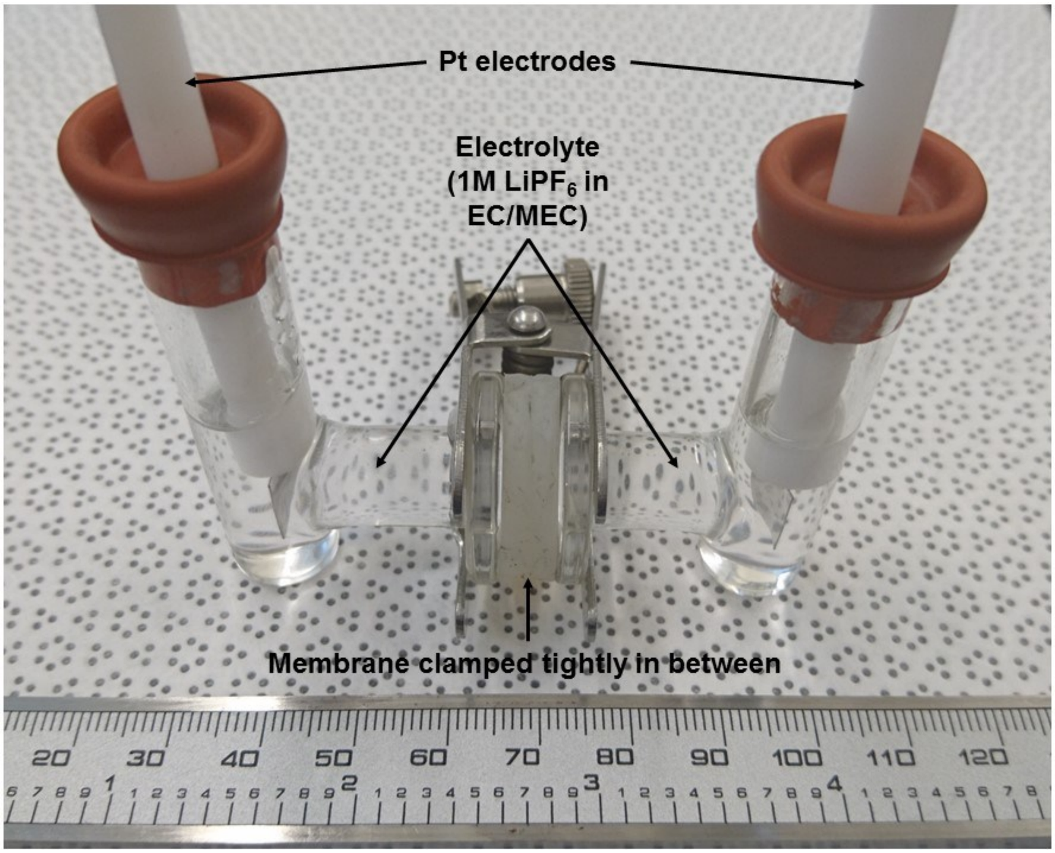

**Fig. S8** Photo of an H-type cell

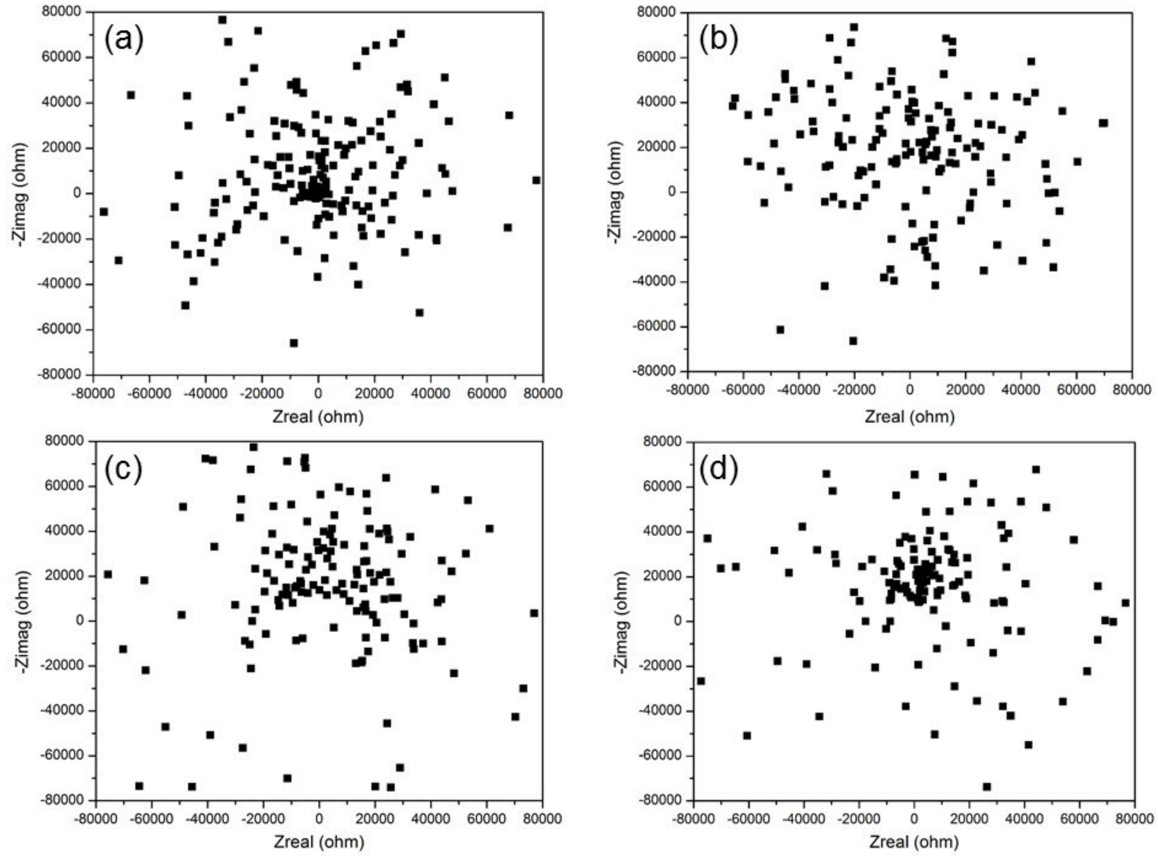

**Fig. S9** AC impedance spectrum of the H-type cell with (a) dense PVDF separator with no lithium ionic conductivity and the non-porous rubber separator after soaking for (b) 0 h, (c) 0.5 h and (c) 1 h.

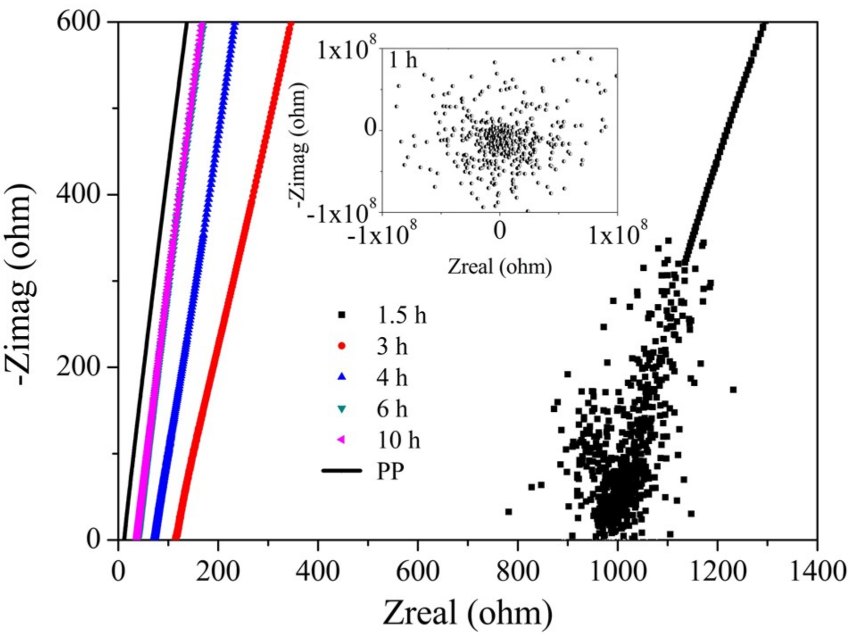

**Fig. S10** AC impedance spectra of sandwich structured stainless steel/separator/staniless steel cells with wetted PP separator and rubber separators swelled for 1 h~10 h.

The impedance spectra change of the rubber separator swelled with soaking time showed the same trend as the results of H-type cell.

The whole cell resistance of the rubber separator based cell (38 Ω) is ~3 times bigger than that of the PP separator based cell (11 Ω). Considering the rubber separator is ~2 time thicker than the PP separator, their ionic conductivities in coin cells are at the same level.

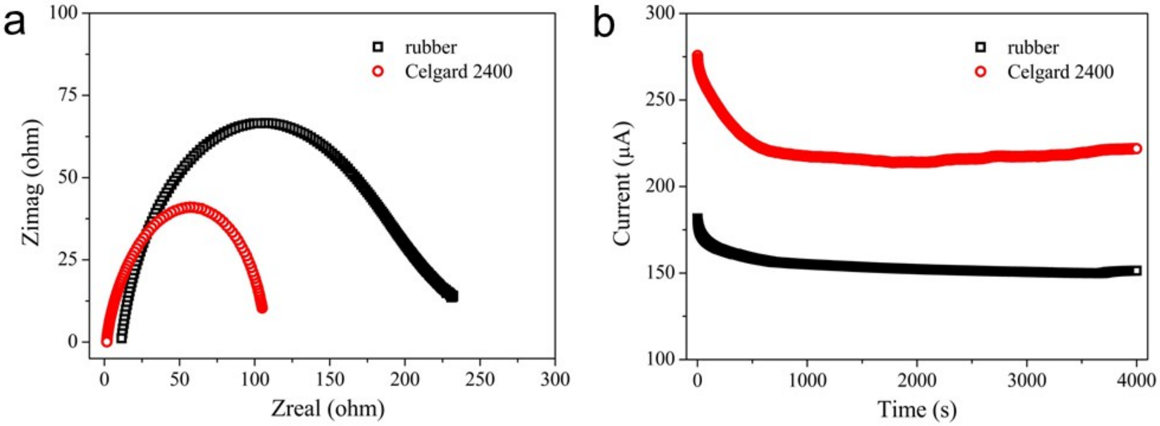

**Fig. S11** The lithium-ion transference numbers test. (a) AC impedance spectroscopy (40~110 MHz) of coin cells employing Celgard 2400 and the rubber separator, respectively. Cells are tested 1 day after assembling. (b) DC polarization curves of the cells. $V_{DC}$=50 mV.

We tested the t+ using the method reported by L. Suo et al [L. Suo et al, Nature Communications, 2013, 4:1481, DOI: 10.1038/ncomms2513]. The Li ion transference number can be calculated as: $t_+=I_{Dc}\times R_{cell}/V_{DC}$, where $V_{DC}$ is the voltage used in DC polarization, $I_{DC}$ is the stable current obtained, and $R_{cell}$ is total resistance of the cell obtained from AC impedance test. For celgard 2400: $I_{DC}$=220 μA, $R_{cell}$=108 Ω; for the rubber separator: $I_{DC}$=151 μA, $R_{cell}$=252 Ω. Then we can get the Li ion transference numbers: $t_{+\ Celgard}$=0.48 and $t_{+\ rubber}$=0.76. As can be seen, the Li ion transference number of the rubber separator is much higher than that of the celgard 2400 separator.

We assume that in the porous celgard 2400, the separator matrix has little chemical interaction with the uptaken liquid organic electrolyte, so the liquid electrolyte inside the pores has the same properties as bulk liquid electrolyte, including $Li^+$ transference number, which is known to be quite low, as a consequence, the wetted celgard separator inside the cell showed a low $t_+$. However, in the rubber separator, the rubber molecule has weakly acidic protons, which would form hydrogen bonds with F atoms in $[PF_6]^-$, so that to some extent confine the movement of the anions and resulting in a higher $t_+$.

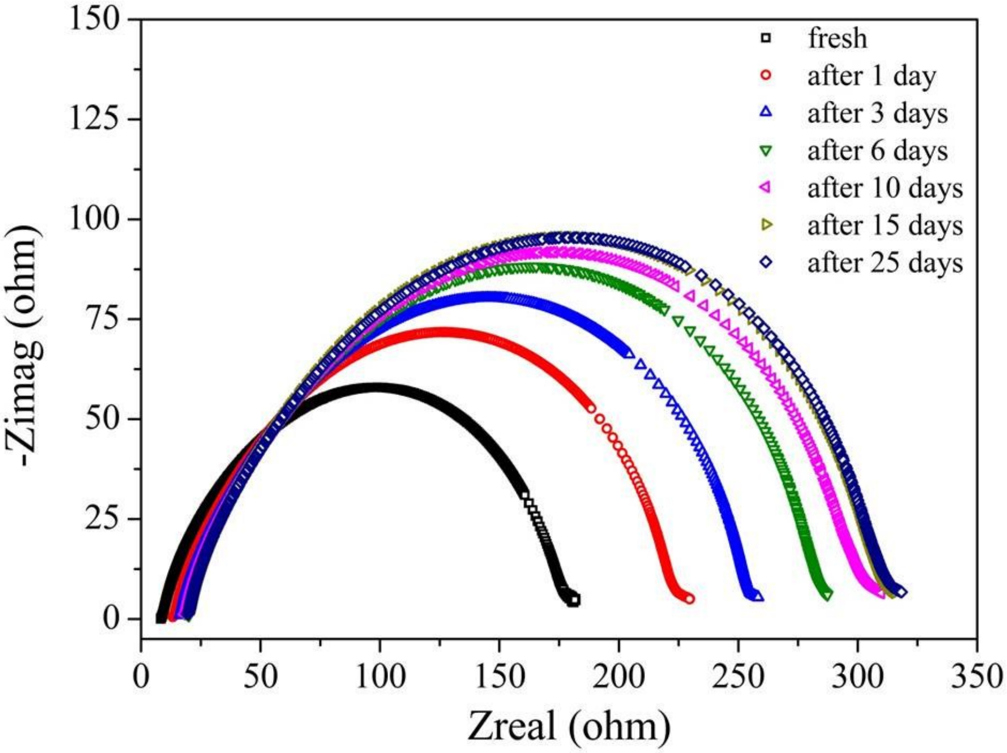

**Fig. S12** Impedance spectra of Li/rubber separator/Li cell

The cell resistance increased with time and leveled off at ~320 Ω after 25 days, which indicates the existance of side reactions between lithium metal and the rubber separator on their interface. However, the resistance and the increase of the resistance are not too large and would not affect the application of the rubber separator seriously.

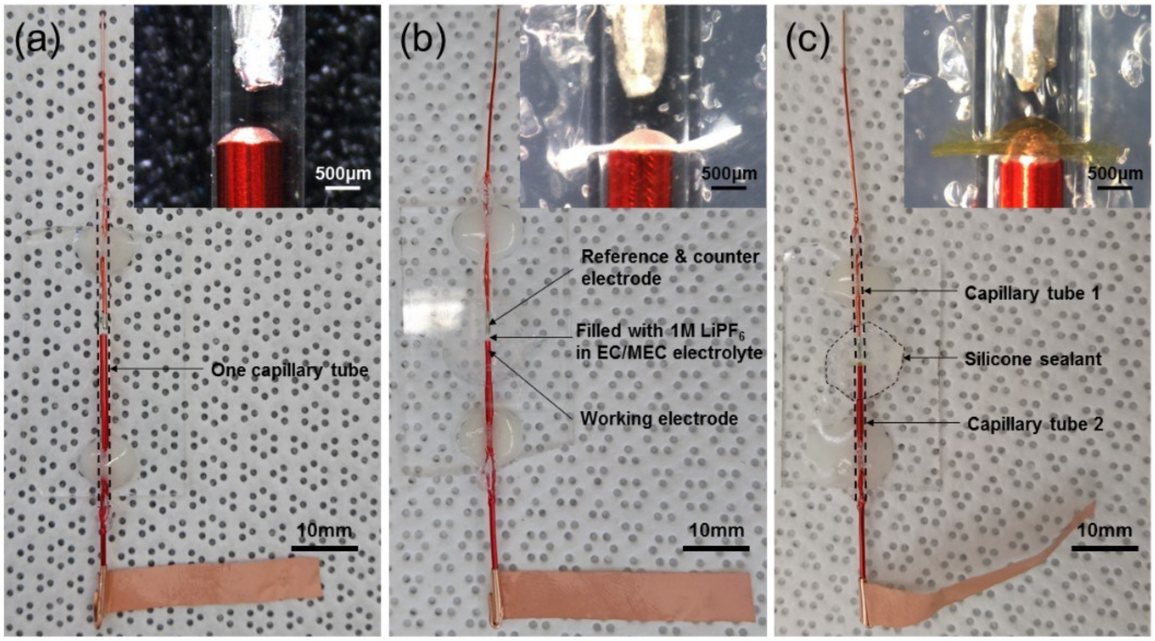

**Fig. S13** Structure of capillary cells with (a) no separator, (b) the porous PP separator and (c) the rubber separator between two electrodes. The insert in each picture is an enlarged view of the electrodes section.

For the cells using a separator, two short capillary tubes were joined together head-to-head with the separator clamped and fixed in between, and the connection was sealed with clear silicone sealant. For the cell without a separator, only one long capillary tube was used. All the capillary cells were fixed on a piece of glass plate. Electrodes and electrolytes were loaded inside a glovebox filled with argon gas. In each cell, a piece of lithium metal was wrapped around an exposed end of a thin enameled copper wire and acted as counter and reference electrodes. A thick enameled copper wire with a round exposed head was used as working electrode. After injection of liquid electrolyte, the open ends of the capillary tubes were sealed and the cells were taken out of glovebox.

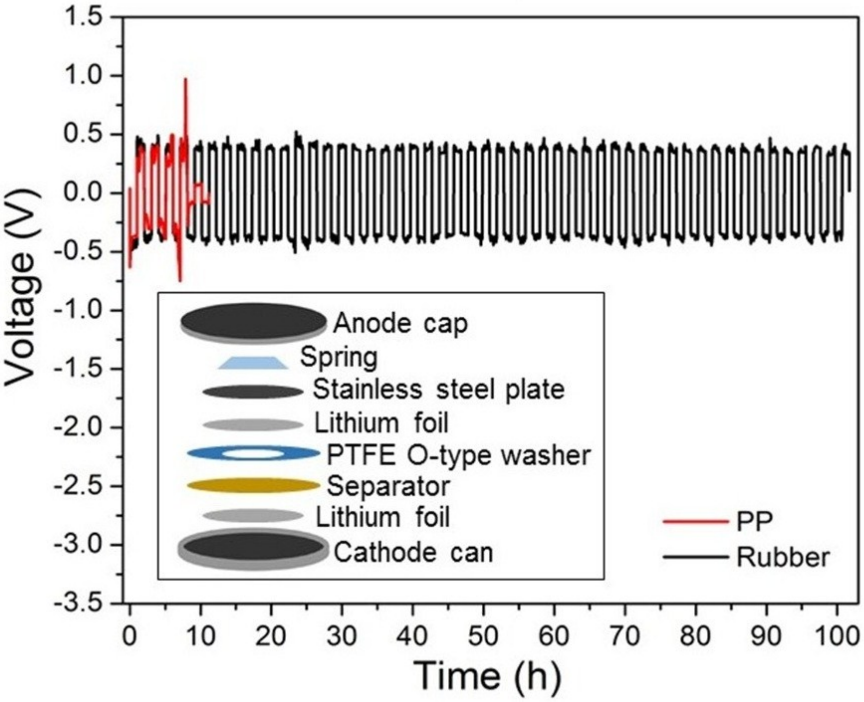

**Fig. S14** Cycling profile of Li-Li symmetrical cells at a current density of 10 mA cm$^{-2}$, and areal capacity of 10 mAh cm$^{-2}$. Insert is the structure of the symmetrical cell. Note that a 50-μm-thick PTFE washer was sandwiched between anode and the separator to fix the position of the separator and reserve space for the lithium anode volume change.

For the cell with porous PP separator, after only 4 cycles, the voltage dropped dramatically, as a result of internal short due to lithium dendrite penetration. In contrast, the cell with our rubber separator was cycled for 50 cycles, and no internal short was observed. Although the Young's modulus of the soft, swollen rubber separator are lower than the 6.8 GPa limit by a factor of $10^4$-$10^5$, it can still prevent the lithium dendrite penetration and survive in large electrode volume change at a high current density of 10 mA cm$^{-2}$ and a high capacity of 10 mAh cm$^{-2}$ for very long time.

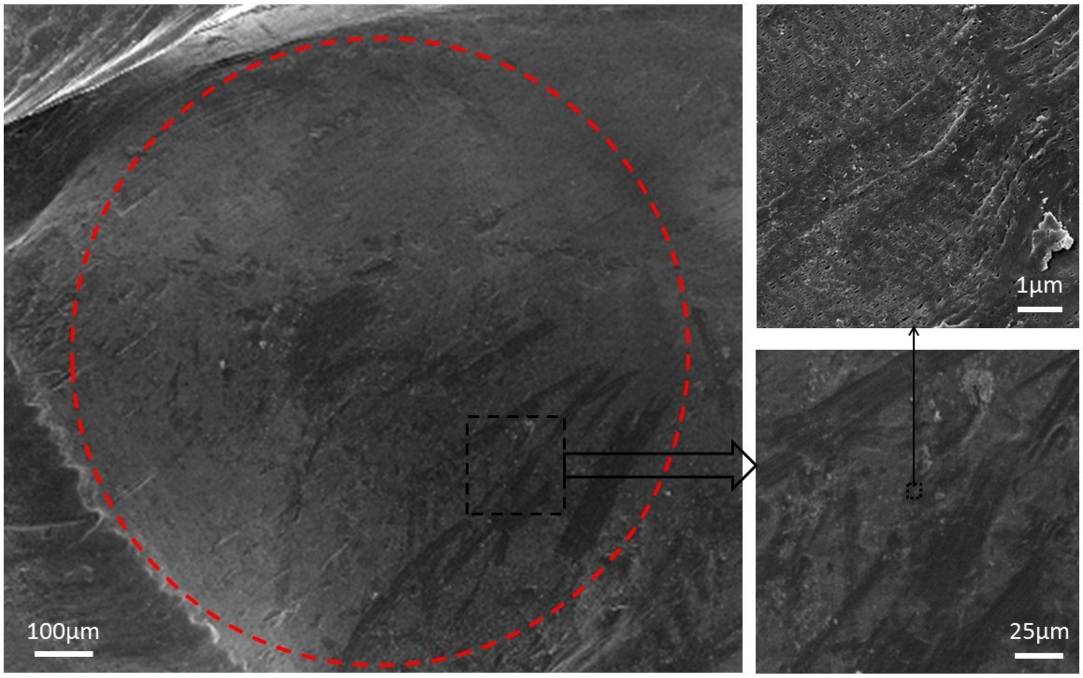

**Fig. S15** SEM images of the PP separator after used in the capillary cell.